Optical and transport properties of heavy fermions: theory compared to experiment

2005 J. Phys.: Condens. Matter 17 2959

(http://iopscience.iop.org/0953-8984/17/19/010)

INSTITUTE OF PHYSICS PUBLISHING JOURNAL OF PHYSICS: CONDENSED MATTER

J. Phys.: Condens. Matter **17** (2005) 2959–2976 doi:10.1088/0953-8984/17/19/010

Optical and transport properties of heavy fermions: theory compared to experiment

N S Vidhyadhiraja[1] **and David E Logan**

University of Oxford, Physical and Theoretical Chemistry Laboratory, South Parks Road, Oxford OX1 3QZ, UK

Received 21 February 2005, in final form 21 February 2005
Published 29 April 2005
Online at stacks.iop.org/JPhysCM/17/2959

Abstract

Employing a local moment approach to the periodic Anderson model within the framework of dynamical mean-field theory, direct comparison is made between theory and experiment for the dc transport and optical conductivities of paramagnetic heavy fermion and intermediate valence metals. Four materials, exhibiting a diverse range of behaviour in their transport/optics, are analysed in detail: CeB_6, $YbAl_3$, $CeAl_3$ and $CeCoIn_5$. Good agreement between theory and experiment is in general found, even quantitatively, and a mutually consistent picture of transport and optics results.

1. Introduction

Heavy electron materials have long been the subject of extensive investigation, for reviews see e.g. [1–7]. Yet in many respects even their 'normal' paramagnetic phase, be it metallic or insulating, has eluded a unified microscopic description on all experimentally relevant temperature (T) and/or frequency (ω) scales. The canonical theoretical model here is of course the periodic Anderson model (PAM). Within the general framework of dynamical mean-field theory [8–11] we have developed in the preceding paper [12] (here referred to as I) a non-perturbative local moment approach to paramagnetic metallic phases of the PAM, with a focus on dc transport and optics; following earlier work on $T = 0$ dynamics [13] and on Kondo insulators [14, 15]. The primary emphasis of I is the Kondo lattice regime relevant to strong correlated heavy fermion (HF) metals. Dynamics/transport on all relevant (ω, T)-scales are encompassed, from the low-energy behaviour characteristic of the lattice coherent Fermi liquid, through incoherent effective single-impurity physics to non-universal high-energy scales. The underlying theory is not however restricted to the Kondo lattice regime, enabling it also to handle e.g. intermediate valence (IV) behaviour.

The present paper is an attempt to provide at least a partial answer to the question: to what extent are the optical and dc transport properties of HF and related materials captured by the PAM and our theory for it? This clearly requires direct, quantitative comparison between theory

[1] Current address: Theoretical Sciences Unit, Jawaharlal Nehru Centre for Advanced Scientific Research, Jakkur, Bangalore-560064, India.

and experiment, which is our purpose here. Specifically, we consider in detail the transport and optics of four materials: CeB_6, $YbAl_3$, $CeAl_3$ and $CeCoIn_5$, all HF metals with the exception of the IV compound $YbAl_3$, and exhibiting a diverse range of behaviour in their transport and optical behaviour. The materials are analysed on a case by case basis in sections 3–6, following a discussion (section 2) of relevant issues involved in making the comparison; we believe it fair to claim that the theory provides a striking account of experiment.

2. Background issues

The Hamiltonian for the PAM is given by equation (2.1) of I, and its physical content is simple: a single correlated f-level in each unit cell hybridizes locally to an uncorrelated conduction band. The model is moreover specified by only four 'bare'/material parameters rendering it minimalist in terms of comparison to experiment—the more so when one recalls that it encompasses regimes of behaviour as diverse as strongly correlated heavy fermion metals and Kondo insulators, intermediate valence, and weak coupling. The dimensionless bare parameters are U, V, ϵ_c and ϵ_f (in units of the conduction electron hopping, $t_* \equiv 1$), with U denoting the local f-level interaction strength and V the local one-electron hybridization coupling an f-level to the conduction band. The energy of the local conduction orbital, ϵ_c, determines the centre of gravity of the free conduction band relative to the Fermi level (and thereby the conduction band filling, n_c), and ϵ_f denotes the f-orbital energy. An equivalent parameter set is U, V, ϵ_c and η, where $\eta = 1 + 2\epsilon_f/U$ specifies the f-level asymmetry.

The non-interacting limit of the model ($U = 0$) is certainly trivial. But in that case—for *all* T—the dc resistivity of the metallic state vanishes, and the optical conductivity contains no absorption below the direct gap except for a δ-function Drude contribution at $\omega = 0$, see I. That this behaviour bears scant comparison to experiment reflects the fact that the essential physics is driven by scattering due to electron interactions. It is of course the latter part, and the resultant many-body nature, of the problem that renders the PAM non-trivial.

In considering dc transport, the first requirement in comparing theory to experiment is thus to extract the contribution ($\rho^{\rm exp}_{\rm mag}(T)$) to the measured resistivity ($\rho(T)$) that isolates the interaction contributions from those of phonons and static impurity scattering. This is given, ideally, by

$$\rho^{\rm exp}_{\rm mag}(T) = \{\rho(T) - \rho(0)\} - \rho_{\rm ph}(T).$$

The first term removes the residual ($T = 0$) resistivity, and hence impurity scattering contribution on the assumption that the latter is T-independent. The second removes the contribution from phonons, usually taken in practice (as assumed in the following) to be the resistivity of the non-magnetic homologue compound with the magnetic ion Ce (or Yb) replaced by La (or Lu), on the assumption that interactions in the latter are negligible. For most systems the phonon contribution is generally negligible for $T \lesssim 50$ K or so.

While this prescription is straightforward in principle, we first deal with a complication that can arise in practice. Experimentally it is the resistance that is measured directly. To convert to a sample independent resistivity requires spatial dimensions to be known with reasonable precision. This does not pose a problem with large crystals, but may do so for small samples. Examples arise in the literature where reported $\rho(T)$s from different groups differ quite significantly; we encounter one such in the case of $CeCoIn_5$ considered in section 6. Absolute resistivities would thus be related to measured values by e.g. $a'\rho(T)$ and $a''\rho_{\rm ph}(T)$, where a' and a'' denote experimental 'mismatch' factors. For comparison to theory (equation (2.2) below) we require, however, only the relative factors a'/a'', to which end we replace the above by

$$\rho^{\rm exp}_{\rm mag}(T) = a\{\rho(T) - \rho(0)\} - \rho_{\rm ph}(T) \tag{2.1}$$

where $a = 1$ in the ideal case (the majority of systems considered below).

The experimental $\rho_{\rm mag}^{\rm exp}(T)$ is to be compared to $\rho_{\rm mag}(T)$ arising from the theory of I for the PAM (where $\rho_{\rm mag}$ was denoted simply by ρ). The system is generically characterized by a low-energy coherence scale $\omega_{\rm L} = ZV^2$, with Z the quasiparticle weight or inverse mass renormalization factor. This scale is a complicated function of the underlying bare parameters, see e.g. [13] and references therein. But in the strong coupling Kondo lattice regime $\omega_{\rm L}$ is exponentially small (because Z is). In consequence, $\rho_{\rm mag}(T)$ exhibits scaling in terms of $\omega_{\rm L}$, i.e. is of form

$$\rho_{\rm mag}(T) = \alpha H\left(\frac{T}{\omega_{\rm L}}\right) \tag{2.2}$$

with the temperature dependence encoded in $T/\omega_{\rm L}$, *independent* of the interaction strength U and hybridization V (α is a trivial overall scale factor, $\alpha \equiv 1/\sigma_0$ in the notation of I); the scaling holding for (any) fixed $\epsilon_{\rm c}$ and η. The scaling resistivity is moreover only weakly dependent on η, and for $T/\omega_{\rm L} \gtrsim 1$–5 or so is in fact independent of $\epsilon_{\rm c}$, reflecting the crossover to incoherent effective single impurity physics (as detailed in I, see e.g. figure 8). This enables direct connection to experiment, via the extent to which the scaling form equation (2.2) captures the T-dependence of experimental resistivities, and indeed also their pressure dependence, for although $\omega_{\rm L}$ will change with pressure the scaling behaviour should remain intact (we consider this explicitly in the case of $CeAl_3$, section 5). Success in this regard also enables $\omega_{\rm L}$ to be determined directly, there being no hope of calculating it '*ab initio*' with any meaningful accuracy. Finally, we add that comparison of theory/experiment proceeds along the same lines away from the asymptotic Kondo lattice regime, in dealing e.g. with intermediate valence materials or intermediate/weak coupling compounds. Here a full parameter set $\epsilon_{\rm c}$, η, U and V must in general be specified, but $\rho_{\rm mag}(T)$ can always be cast in the form of equation (2.2), and appropriate comparison can be made.

Although our comments above focus on static transport, a central purpose of the paper is also to make direct comparison between experiment and theory for optics, on all experimentally relevant frequency and temperature scales. Given prior analysis of dc transport, the underlying model/material parameters are known, either wholly or in part. There is then little room for manoeuvre; the resultant theory either captures the optical behaviour or not, providing a further and quite stringent test of the model's material applicability.

The main physical effect omitted in the PAM itself is that of crystal electric fields (CEFs). The atomic levels of e.g. Ce^{3+}, $^2F_{5/2}$, are generically split into three doublets, the excited levels lying above the ground state by Δ_1, Δ_2. For sufficiently low T only the lowest level matters, it being this alone the PAM seeks to capture. Although the material specific Δ_i are usually larger than $\omega_{\rm L}$ (itself typically $\sim$10–100 K), they often lie in the interval $\lesssim$300 K. Their qualitative influence on dc transport is clear, for additional conduction channels are opened up in accessing higher CEF levels with increasing T. Quantitatively however, the effect is hard to gauge *a priori*, its magnitude naturally depending on how effectively the higher CEF levels couple to the conduction band. Where present and effective, we can expect to see it as a decrease in the experimental resistivity below that predicted by the one-channel PAM, the onset of the deviation appearing at $T \sim \Delta_1$. We add here that while the role of CEF effects has been studied in the context of *single*-impurity Anderson/Kondo models [16–20], with application to lattice-based systems for sufficiently high temperatures where lattice coherence can be neglected, we are not aware of corresponding work in the context of lattice-fermion models.

Finally, we note that our comparison of theory/experiment for Kondo insulators in [15] was free from most of the considerations above. There, theory was compared directly to the experimental $\rho(T)$, for several reasons. First, in contrast to the case of heavy fermion metals, resistivities of the non-magnetic homologues are sufficiently small compared to those of the

Kondo insulating material that $\rho_{\rm ph}(T)$ in equation (2.1) can be neglected with impunity. This in turn means that any sample geometry factor $a \neq 1$ in equation (2.1) can simply be absorbed into the overall scale factor α (equation (2.2)), so any lack of precision in obtaining $\rho(T)$ is immaterial. The role of impurities is also different in Kondo insulators. In metals this arises from static impurity scattering, presumed to be T-independent and generating the finite residual resistivity $\rho(0)$, which is thus subtracted out as in equation (2.1). In Kondo insulators by contrast, $\rho(T)$ diverges as $T \to 0$, reflecting the insulating ground state. This occurs even in the presence of localized impurity states in the $T = 0$ insulating gap, which generate conduction by variable-range hopping, generally operative over a narrow T-interval (e.g. $\lesssim$8 K for SmB_6 [15, 21]), and whose net effect on $\rho(T)$ at temperatures above this interval (where direct comparison is made to experiment) is usually sufficiently small to be neglected.

We turn now to comparison with experiment for the metallic heavy fermion and intermediate valence materials considered.

3. CeB_6

Among the rare-earth hexaborides, the Kondo insulator SmB_6 and the heavy fermion compound CeB_6 have been investigated for many years [1, 7, 22–26]. The former was considered in our recent work [15] on the particle–hole symmetric PAM. There it was shown that a single low-energy (indirect gap) scale underlies the temperature dependence of both the static and optical conductivity, and (with minimal input of bare material parameters) the frequency dependence of the optics as well. Here we consider its metallic counterpart CeB_6, likewise a cubic system [22]. At the lowest temperatures, various antiferromagnetic phase transitions occur between $T \sim 1.6$–3.3 K [22, 24, 26], above (and below) which the paramagnetic phase arises, 'phase-I' for $T > 3.3$ K.

The relative ease with which large, clean single crystals of CeB_6 can be grown (see e.g. [26]) has been a motivating factor in its investigation. The dc resistivity has been measured by several groups (e.g. [22, 26]) and since the sample quality is in general good, the residual resistivity is very small. In addition, the relatively large crystal sizes imply small errors in sample geometry, hence the factor a in equations (2.1) can safely be assumed to be 1. The phonon contribution to the resistivity is as usual taken as the resistivity of the non-magnetic homologue LaB_6 [22], the latter having the same lattice structure with similar lattice parameters and phonon dispersion as CeB_6 (from inelastic neutron scattering [22]). The experimental magnetic resistivity $\rho^{\rm exp}_{\rm mag}(T)$ is then readily obtained [22], and shown in figure 1 (we add that the phonon contribution kicks in only for $T \gtrsim 50$ K, so the magnetic resistivity essentially coincides with the raw resistivity at lower temperatures). A small kink arises in $\rho^{\rm exp}_{\rm mag}(T)$ at $T \sim 3.3$ K, reflecting the transition from the paramagnetic phase I to phase II [22, 26] mentioned above. The experimental resistivity is seen to exhibit the classic 'shape' for a strongly correlated HF metal, increasing from zero at $T = 0$ and going through a coherence peak at $T \sim 4$ K, before decreasing through a small log–linear regime (similar to that shown in figure 6(a) of I) to a shallow minimum at $T \sim 375$ K, increasing thereafter at higher temperatures where it shows conventional metallic behaviour.

To compare $\rho^{\rm exp}_{\rm mag}(T)$ to theory, first recall from I that the asymptotic scaling resistivity $\rho_{\rm mag}(T)$ is a universal function of $T/\omega_{\rm L}$ for fixed $\epsilon_{\rm c}$ and η (being independent of the local interaction U and hybridization V), see e.g. figure 8 of I. For a chosen $(\epsilon_{\rm c}, \eta)$ the scaling $\rho_{\rm mag}(T)$ is then straightforwardly superposed onto $\rho^{\rm exp}_{\rm mag}(T)$ with an appropriate rescaling of the temperature and resistivity axes, thus enabling the low-energy scale $\omega_{\rm L}$ to be determined. The asymptotic scaling $\rho_{\rm mag}(T)$ is shown in figure 1 (dotted line) for a moderate $\epsilon_{\rm c} = 0.5$ and $\eta = 0$, with the resultant coherence scale thereby found to be $\omega_{\rm L} \simeq 5.5$ K. It is seen to capture

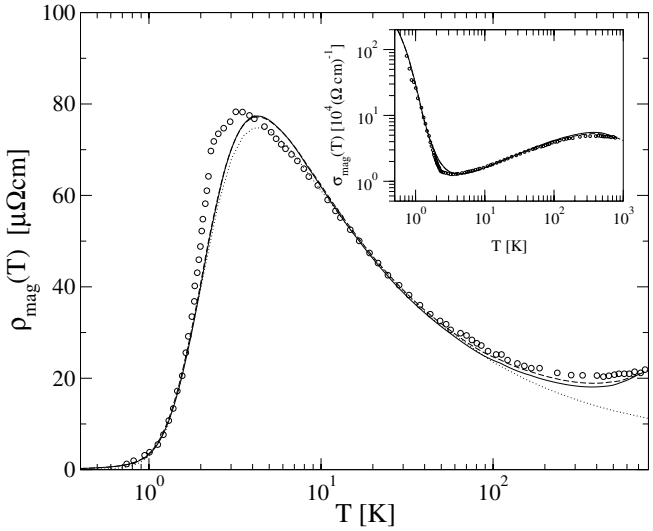

Figure 1. Comparison of experimental $\rho^{\rm exp}_{\rm mag}(T)$ (circles) for CeB_6 [22] to theory, on a log–linear scale. The solid curve shows $\rho_{\rm mag}(T)$ for $U = 4.75$, $V^2 = 0.4$, while the dashed curve is for $U = 2.45$, $V^2 = 0.2$; both theory sets have common $\epsilon_{\rm c} = 0.5$, $\eta = 0$ and the same $\omega_{\rm L} = 5.5$ K. The dotted curve shows the asymptotic scaling resistivity. Inset: the dc conductivity $\sigma_{\rm mag}(T) \equiv 1/\rho_{\rm mag}(T)$ on a log–log scale.

the experimental resistivity up to $T \simeq 100$ K, but above this it deviates below experiment, continuing as it must to decrease monotonically (see figure 8 of I) and hence lacking the minimum occurring experimentally for CeB_6 at $T_{\rm min} \simeq 375$ K, i.e. $\tilde{T}_{\rm min} = T_{\rm min}/\omega_{\rm L} \simeq 70$.

As discussed in I (figure 8 inset), the latter behaviour is physically natural and readily encompassed theoretically. No real HF material is in the universal scaling regime 'for ever'—it must be exited sooner or later with increasing T. Deviation of $\rho_{\rm mag}(T)$ from its asymptotic scaling form at sufficiently high temperatures signifies the onset of non-universality, and the location of the non-universal minimum in $\rho_{\rm mag}(T)$ provides an opportunity to identify the ratio U/V^2 of the effective bare material parameters, which will be helpful in making a prediction for the ω-dependence of the optical conductivity $\sigma(\omega; T)$. Specifically, for the chosen $\epsilon_{\rm c} = 0.5$, $\eta = 0$, we find that the theoretical $\rho_{\rm mag}(T)$ indeed has a minimum at $\tilde{T}_{\rm min} \simeq 70$ (as in experiment) for $U/V^2 \simeq 12$. This is illustrated in figure 1, where we show the resultant theoretical $\rho_{\rm mag}(T)$ for $U = 4.75$, $V^2 = 0.4$ (solid curve) and $U = 2.45$, $V^2 = 0.2$ (dashed curve). The two $\rho_{\rm mag}(T)$s barely differ from the asymptotic scaling resistivity for $T \lesssim 100$ K, are essentially coincident with each other across the entire T-range, and each possesses a weak minimum at $T \simeq 375$ K. Except naturally for a small neighbourhood around the low-temperature phase transitions (which the theory does not seek to address), the resultant theoretical $\rho_{\rm mag}(T)$ is seen to be in rather good agreement with experiment, as evident further from the inset to figure 1 where the corresponding dc conductivity $\sigma_{\rm mag}(T)$ is shown. A CEF excitation is known to occur at $\sim$2.5 meV (30 K) [27] (with a second lying at a much higher energy, 46 meV [27]), but as judged from the above comparison this appears to play a minor role in the dc transport itself.

To determine the optical conductivity on all ω-scales, including non-universal frequencies, requires U and V^2 to be separately specified, as discussed in I. This is clearly not provided by the above analysis, but a reasoned prediction for $\sigma(\omega; T)$ may nonetheless be made. For

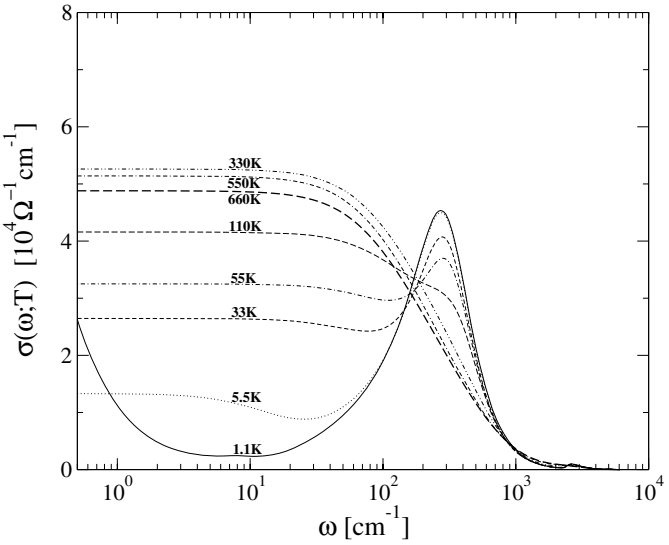

Figure 2. Predicted optical conductivity of CeB_6: $\sigma(\omega; T)$ versus ω in cm^{-1} at temperatures $T = 1.1$, 5.5, 33, 55, 110, 330, 550 and 660 K.

fixed $U/V^2 \simeq 12$ as above, we find that varying U across the range ∼2.5–5 produces only a modest change in both the ω- and T-dependence of $\sigma(\omega; T)$, leading in particular to a direct gap absorption lying in the interval ∼200–300 cm^{-1}, as well as a quasiparticle weight Z of the order of 10^{-2} that is consistent with the effective mass $(m^*/m_e \equiv)\ m^* \simeq 100$ deduced from the specific heat coefficient $\gamma = 250$ mJ mol^{-1} K^{-2} measured for phase I of CeB_6 [22, 26]. In other words, on the assumption that the reasonably wide U-range above encompasses the behaviour of CeB_6, the optics are relatively insensitive to the precise value of U.

To this end we show in figure 2 the predicted optical conductivity for $U = 2.45$, $V^2 = 0.2$, with the ω/ω_L-dependence of the theoretical $\sigma(\omega; T)$ converted to ω in cm^{-1} using $\omega_L = 5.5$ K$(\equiv 3.8\ cm^{-1})$ deduced from the above analysis of the dc resistivity, and with $\sigma(\omega; T)$ shown for a range of temperatures from 1.1 to 660 K. As $\omega \to 0$, the T-dependence of the dynamical conductivity follows the dc values shown in the inset to figure 1. At the lowest temperature $T = 1.1$ K $\simeq \omega_L/5$ an emergent low-frequency Drude absorption on frequency scales $\omega \lesssim 1\ cm^{-1}$ is evident in $\sigma(\omega; T)$ (see also figure 9 of I), separated by a clear optical pseudogap centred on $\omega \approx 10\ cm^{-1}$ from a strong direct gap absorption centred on $\omega \sim 250\ cm^{-1}$. The Drude absorption is rapidly suppressed on increasing T, being all but dead by $T \sim \omega_L = 5.5$ K, while the optical pseudogap is progressively 'filled in' on temperature scales set by ω_L. The direct gap absorption is largely unaffected by temperature until $T \gtrsim$ (5–10)ω_L or so, but is significantly eroded by $T \sim 110$ K and in essence destroyed by room temperature.

The optical conductivity of CeB_6 has in fact been measured by Kimura *et al* [23], but only in the frequency interval 50 meV $\simeq 400\ cm^{-1}$ to 10 eV $\simeq 8 \times 10^4\ cm^{-1}$, and at a temperature of 300 K. No strong direct gap absorption was observed, itself suggesting that the absorption occurs at frequencies of the order of $\omega \sim 200\ cm^{-1} \simeq 300$ K or less; instead a broad, featureless and monotonically decreasing spectral lineshape was found. This is of course consistent with the prediction from figure 2 that the direct gap peak is almost completely washed away at room temperature. In order to observe non-trivial ω- and T-dependence in the optical conductivity of CeB_6, we thus suggest the frequency domain be extended down to

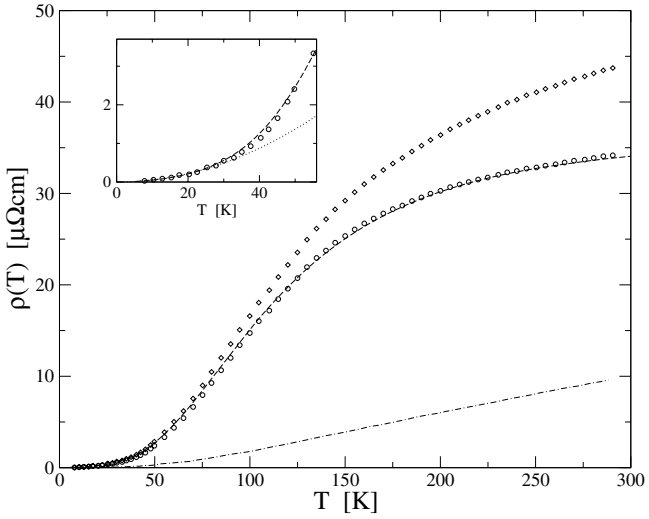

Figure 3. The dc resistivity of $YbAl_3$ (diamonds) and $LuAl_3$ (point–dash line), from [28] with the small residual resistivity subtracted. The experimental $\rho^{\rm exp}_{\rm mag}(T)$ (circles) is obtained by subtracting $\rho(T) - \rho(0)$ for $LuAl_3$ from that for $YbAl_3$. The theoretical $\rho_{\rm mag}(T)$ (dashed line) is obtained for $\epsilon_{\rm c} = 0.5$, $\eta = 1.2$, $U = 4.9$, $V^2 = 0.8$, and superimposed on $\rho^{\rm exp}_{\rm mag}(T)$ with $\omega_{\rm L} = 254$ K. The level of agreement between theory and experiment is clear. Inset: the low temperature behaviour; including (dotted line) a fit to the asymptotic Fermi liquid form $\rho_{\rm mag}(T) \propto T^2$, which is seen to persist in both experiment and theory up to $T \sim 30$ K.

$\sim$10 $\rm cm^{-1}$ (or lower to observe the Drude absorption), and that experiments be performed at considerably lower temperatures, such as those shown in figure 2.

4. $YbAl_3$

Our main focus in I and [13] has been the strongly correlated heavy fermion regime where the f-level $\epsilon_{\rm f} \ll 0$ lies well below the Fermi level, with $\epsilon_{\rm f} + U \gg 0$ well above it, such that the f-electrons are essentially localized, $n_{\rm f} \to 1$. The underlying local moment approach is not however restricted to the Kondo lattice regime, and in particular can also readily handle IV behaviour. In this case, depletion for example of $n_{\rm f}$ from unity reflects the fact that $\epsilon_{\rm f}$ lies relatively close to the Fermi level, such that the appropriate $\eta = 1 + 2\epsilon_{\rm f}/U$ regime is $\eta \approx 1$.

The compound $YbAl_3$, which crystallizes in a simple cubic Cu_3Au-type structure and does not order magnetically [28], provides a prime example of IV behaviour. Figure 3 shows the experimental dc resistivity of $YbAl_3$, and its non-magnetic homologue $LuAl_3$, at ambient pressure (data from [28] with the tiny residual resistivity subtracted). The resultant magnetic resistivity $\rho^{\rm exp}_{\rm mag}(T)$ is also shown in figure 3, obtained simply by subtracting the resistivity of $LuAl_3$ from that of $YbAl_3$ (the samples [28] are high quality single crystals, hence the factor a in equation (2.1) is taken as unity). $\rho^{\rm exp}_{\rm mag}(T)$ is seen to increase monotonically with T, lacking the coherence peak seen in strongly correlated HF materials. This behaviour is characteristic of IV [29], as too is e.g. the low/moderate effective mass in the range $m^* \sim$ 15–30 inferred from dHvA [30], optical [31] and specific heat [32] measurements, and the Yb mean valence $z_{\rm v} \equiv 2 + n_{\rm f}$ is estimated experimentally as $z_{\rm v} \sim$ 2.65–2.8 [32, 33].

In the strongly correlated HF regime, physical properties such as $\rho_{\rm mag}(T)$ exhibit scaling as a function of $T/\omega_{\rm L}$, independent of the interaction U and hybridization V as detailed in

I, occurring formally for all T/ω_L in the asymptotic strong coupling limit, and in material practice over a significant albeit naturally finite T/ω_L range as seen above for CeB_6 (and in [15] for Kondo insulators). This is *not* by contrast the case in the IV regime, and neither is it to be expected. Here the 'full set' of bare/material parameters η, ϵ_c, U and V must be specified. To compare theory to experiment for $YbAl_3$ we consider a moderate $\epsilon_c = 0.5$ with $\eta = 1.2$, $U = 4.9$ and $V^2 = 0.8$; corresponding to a modest interaction strength $U/\pi\Delta_0 = 1.4$ (with $\Delta_0 = \pi V^2 \rho_0(-\epsilon_c)$ as in I) and an $\epsilon_f = 0.49$ close to the Fermi level ($\epsilon_f/\Delta_0 = 0.44$). The resultant f-band filling is found to be $n_f \simeq 0.65$ ($z_v \simeq 2.65$), consistent with the mixed valence nature of $YbAl_3$, and a quasiparticle weight $Z \simeq 0.05$ is found, implying an effective mass $m^* \simeq 20$ that is likewise consistent with experiment as above.

The theoretical dc resistivity $\rho_{mag}(T)$ versus T/ω_L for these parameters has been determined, and superposed onto the experimental $\rho^{exp}_{mag}(T)$ in the usual way. The resultant low-energy scale is found thereby to be $\omega_L = 254$ K, and comparison between theory and experiment is shown in figure 3. The agreement is clearly excellent, for all temperatures. The inset to figure 3 shows the low temperature behaviour on an expanded scale, together with a fit (dotted line) to the $T \to 0$ Fermi liquid form $\rho_{mag}(T) \propto T^2$. As known from experiment [32], and seen also in the present theory, this asymptotic form is seen to persist up to a temperature 'T_{FL}'~ 30 K that is an order of magnitude lower than $\omega_L \sim 254$ K, and about which fact we make two brief comments. First, to emphasize that this arises naturally here within a theoretical approach to the periodic Anderson model itself (with no appeal e.g. to calculations based upon a single-impurity Anderson model [32]). Second, the quantitative distinction between 'T_{FL}' and ω_L is in our view to be anticipated, for ω_L is the natural low-energy scale in the problem, and since $\rho(T) \propto T^2$ is the *asymptotic* $T \to 0$ behaviour, we would as such expect it to arise only for $T \ll \omega_L$.

While the experimental data shown in figure 3 extend up to $T \simeq 300$ K, the theoretical $\rho_{mag}(T)$ may be used to predict the full $\rho(T)$ for $YbAl_3$ over a much larger temperature interval. To that end we simply calculate $\rho_{mag}(T)$ at higher T, and add to it the resistivity of $LuAl_3$ representing the phonon contribution, itself extended to higher T by linear extrapolation of the Lu data in figure 3 (point–dash line, and which extrapolation is clearly warranted). The resultant $\rho(T)$ is shown in figure 4 out to $T = 800$ K, and we note that it continues to increase monotonically above 300 K, precluding as such the occurrence of a coherence maximum at a T in excess of that shown in figure 3. Experimental results for $\rho(T)$ up to $T \simeq 750$ K have in fact been reported [34]. This data does not appear to be quite as clean as that of [28] in the interval 50 K $\lesssim T <$ 300 K, but for $T \lesssim 50$ K the $\rho(T)$ from [34] collapses very well onto that of [28] (considered above) with an overall ρ-axis rescaling factor $a = 1.2$ (equation (2.1)). Taking this a, the resultant $\rho(T)$ from [34] is shown in figure 4 in the temperature interval 300–750 K, and is seen to agree well with the theoretical result.

We turn now to the optical conductivity of $YbAl_3$, which has only recently been measured at infrared frequencies and below [31]. This is reproduced in the top panel of figure 5, from which three key features are evident [31]: the low-frequency Drude response characteristic of the free carriers; a depleted pseudogap occurring at low temperatures (at $\omega \sim 20$ meV) and flanked on its right by a shoulder at $\omega \sim 50$–60 meV; followed by the broad, strong direct gap (or mid-infrared, mIR) peak centred near $\omega \sim 250$ meV.

The bottom panel in figure 5 shows the theoretical optical conductivity at the same temperatures and on the same frequency scale as experiment, obtained using the same bare parameters employed in figures 3, 4, and with $\omega_L = 254$ K as deduced above; in other words with no additional input other than that inferred from the dc transport comparison. Barring a mismatch in the relative intensity of the direct gap peak on which we comment below, the agreement between theory and experiment is seen to be rather good in terms of the pseudogap

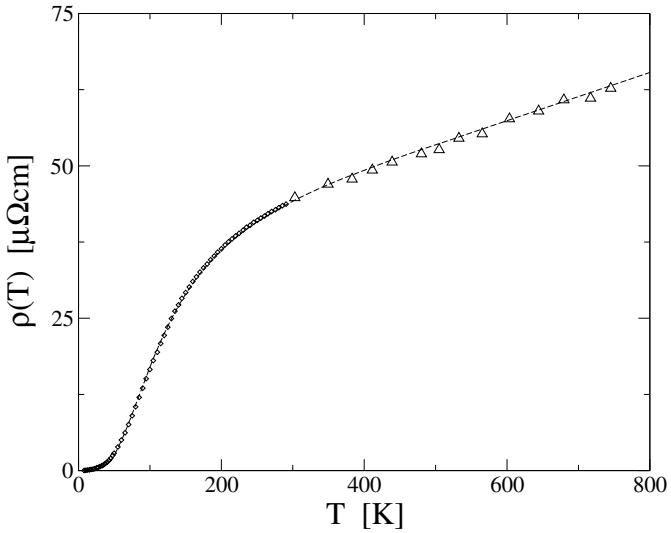

Figure 4. Theoretical $\rho(T)$ for $YbAl_3$ (dashed line) up to 800 K, compared to the experimental results of [28] (diamonds) up to $T = 300$ K and of [34] from 300 to 750 K (triangles), as detailed in text.

structure, the shoulder, the position and width of the mIR peak, and the thermal evolution of the optical conductivity. The shoulder in particular merits comment, being a distinct spectral feature that is thermally destroyed with increasing temperature [31]. It has been speculated in [31] (not unreasonably) that its origin may lie outside the scope of the PAM and/or be material specific. The present results however suggest the contrary. Theoretically, we find that the existence of the shoulder shown in figure 5 is not specific to the particular set of bare material parameters considered, but rather characteristic of IV in general terms—a clear optical shoulder arising in the vicinity of $\omega \simeq 2$–$3\omega_{\rm L}$ as the bare parameters are varied over quite a significant range. Its origins reflect the underlying behaviour of the f-electron self-energy, and we do not therefore have a simple physical explanation for it; but neither do we doubt its generic occurrence. For the case of $YbAl_3$, with $\omega_{\rm L} \sim 250$ K deduced from dc transport as above, the shoulder thus lies at $\omega \sim 50$ meV as indicated by the vertical arrows in figure 5 and agreeing rather well with experiment.

Finally, we comment on the mismatch in the vertical (intensity) axes in figure 5. The theoretical $\sigma(\omega; T)$ represents of course the conductivity in the absence of phonons, which inevitably introduces a certain mismatch between theory and experiment as $\omega \to 0$ at temperatures high enough for the phonons to kick in, but the phonon background would not extend up to mIR frequencies, so the intensity of the direct gap peak in theory and experiment should agree. The fact that it does not could obviously mean that a different bare parameter set may be more appropriate than that identified here. Alternatively, the issue may be experimental. The $\sigma(\omega; T)$ spectra are obtained [31] via a Kramers–Krönig transformation of the total reflectance between 7 meV and 35 eV, with a Hagen–Rubens formula used for low-energy extrapolation, and with several spectrometer sources employed in different frequency intervals, which require matching using appropriate constant factors (see e.g. [35]). This is intricate, and there is undoubtedly the possibility of error in determining the absolute intensity of the direct gap. A surface impedance probe such as the one used in [35] might be able to resolve the matter, while if the issue is not experimental then a more extensive scan of the bare

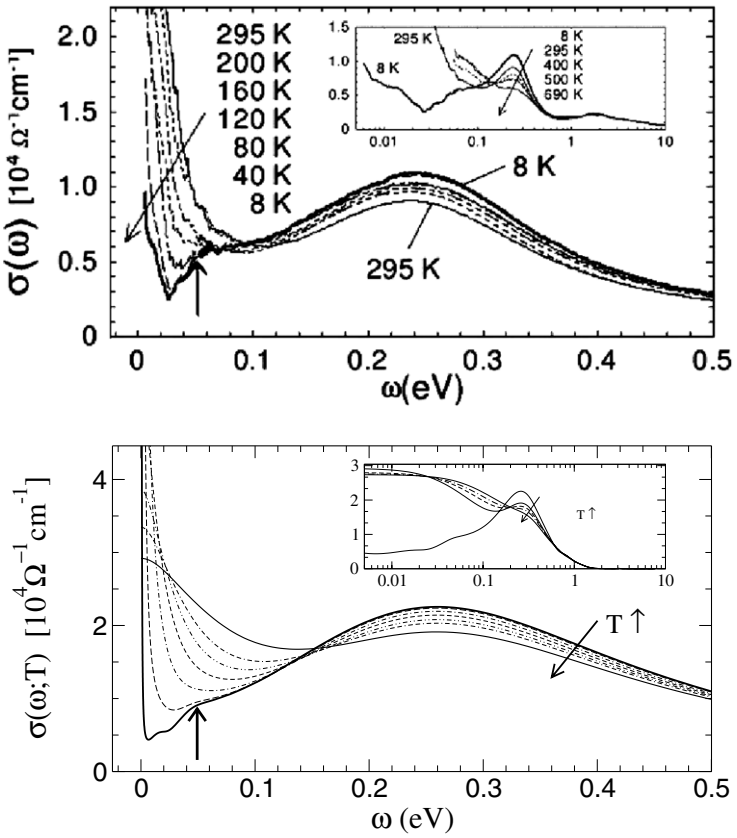

Figure 5. Top panel: experimental optical conductivity of $YbAl_3$ [31]. Bottom panel: theoretical $\sigma(\omega; T)$ for the same parameters as in figure 3, at the same temperatures and on the same frequency scale as in experiment. The vertical arrow in both panels indicates the position of the theoretically predicted shoulder, at $\omega \simeq 2\omega_L \sim 50$ meV. The insets show the thermal evolution of $\sigma(\omega; T)$ for higher temperatures. The overall experimental lineshape including the pseudogap, shoulder and mIR peak, as well as their thermal evolution, is well reproduced by theory.

parameter space is required. That notwithstanding, however, the present theory does appear to provide a remarkably consistent description of both transport and optics in $YbAl_3$.

5. $CeAl_3$

The classic system $CeAl_3$ has long been subject to extensive investigation, see e.g. [1, 35–42]. In contrast to its Yb cousin considered above, $CeAl_3$ is a prototypical heavy fermion material, as attested for example by the large specific heat coefficient $\gamma \sim 1.4 \times 10^3$ mJ mol^{-1} K^{-2} [39] and corresponding effective mass $m^* \sim 700$ [35, 39].

A helpful starting point for comparison of theory to experiment is a rough knowledge of the parameter regime to which the system belongs. In the case of $CeAl_3$ we can glean such information from the unusual behaviour of the experimental optical conductivity [35], which is shown in the top panel of figure 7 below. Typical features found in optical lineshapes of HF systems are the Drude peak at low frequencies, followed by a pseudogap, with a strong direct gap (or mIR) absorption at higher frequencies (see e.g. figures 2, 5, 10). In the case of $CeAl_3$ however, while the Drude peak is clearly evident at low T, a distinct pseudogap

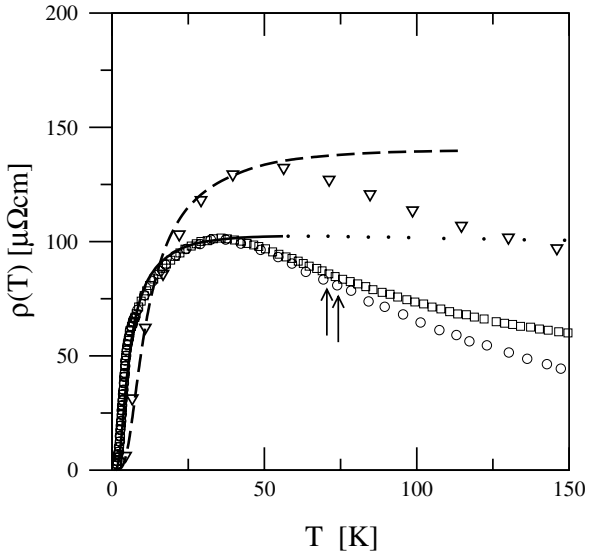

Figure 6. dc resistivity of $CeAl_3$ at ambient pressure (squares, from [37] with the residual resistivity subtracted), and the corresponding magnetic resistivity $\rho^{\rm exp}_{\rm mag}(T)$ (circles) [37]. The theoretical $\rho_{\rm mag}(T)$ for $\epsilon_{\rm c} = 1.5$, $\eta = 0$ is shown by the solid/dotted line, the resultant coherence scale being $\omega_{\rm L} = 33$ K. The agreement between theory and experiment is good for $T \lesssim 45$ K, beyond which deviations naturally occur due to the presence of two crystal field split levels at 6.1 meV (71 K) and 6.4 meV (75 K) [40], marked by arrows. Triangles denote $\rho^{\rm exp}_{\rm mag}(T)$ for $CeAl_3$ at a higher pressure $P = 0.4$ GPa [38]. The dashed line shows the same theoretical curve as used for comparison to the ambient pressure data, but with simple rescaling of the axes, leading to $\omega_{\rm L}(0.4\ {\rm GPa}) = 71$ K.

and the mIR peak are absent. In fact there is little frequency dependence beyond the Drude absorption range.

From our theoretical work in I we know that increasing $\epsilon_{\rm c}$, and hence reducing the conduction band filling $n_{\rm c}$, acts to diminish the pseudogap (see inset to figure 10 of I); relatedly, it also tends to suppress the direct gap absorption, suggesting that a suitably large $\epsilon_{\rm c}$ is required for $CeAl_3$. However this by itself is not sufficient: a large $\epsilon_{\rm c}$, but with a modest hybridization V between the f-levels and the conduction band, can still give rise to a distinct mIR absorption. A suitably large hybridization thus also seems necessary to suppress strongly the direct gap absorption. Unusually large CEF parameters found in inelastic neutron scattering experiments have in fact also been attributed to a large hybridization V [40], supporting this inference. And from the large effective mass mentioned above, we know the system is in the strong correlated Kondo lattice regime, requiring a significant interaction strength U.

The picture of $CeAl_3$ thus suggested is of a system with low conduction band filling $n_{\rm c}$ (large $\epsilon_{\rm c}$), a significant hybridization V, and strong local interactions. We have investigated this regime in some detail, and for comparison to transport and optical experiments on $CeAl_3$ will consider explicitly the following material parameters: $\epsilon_{\rm c} = 1.5$ and $\eta = 0$ (results are quite insensitive to η in the Kondo lattice regime), together with $V^2 = 1.4$ and $U = 6.9$ (or $U/\pi\Delta_0 \simeq 8.4 \gg 1$ signifying strong correlations, where $\Delta_0 = \pi V^2 \rho_0(-\epsilon_{\rm c})$ as in I). Additional specification of U and V^2 is of course required in order to consider the optical conductivity on all frequency scales, whereas $\epsilon_{\rm c}$ and η alone suffice to determine the dc resistivity in the scaling regime. With these parameters we find a quasiparticle weight $Z \simeq 1.6 \times 10^{-3}$ and hence an effective mass $m^* \simeq 625$, in good agreement with $m^* \simeq 690$ deduced from specific heat measurements [35, 39]. The resultant conduction band filling

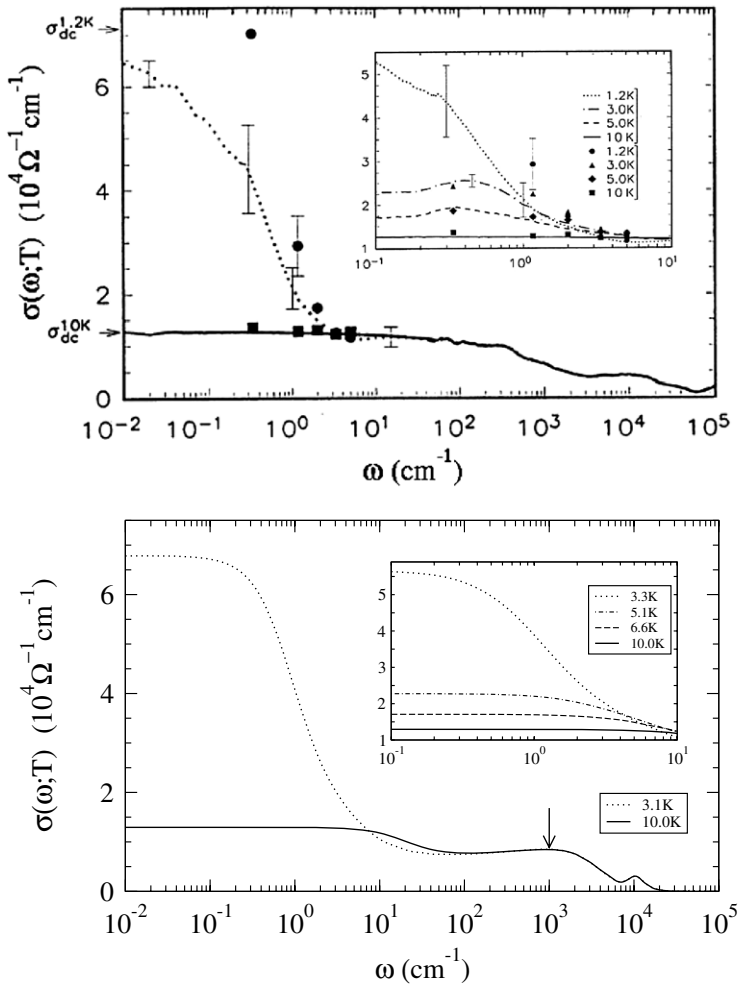

Figure 7. Top panel: experimental optical conductivity of $CeAl_3$ at the temperatures indicated, from [35]. Bottom panel: theoretical $\sigma(\omega; T)$. Discussion in text. The vertical arrow denotes the location of the direct gap, where a mIR peak is usually found for other HF systems.

is $n_c = 0.17$, while the f-level occupancy $n_f = 1.0$, consistent with the firmly trivalent ($z_v \equiv 4 - n_f$) nature of the Ce ion expected in the HF regime.

We first consider dc transport measurements. These have been obtained by several groups [35, 37–39, 41], which we find in general concur well on subtraction of appropriate residual resistivities (so $a = 1$ is taken in equation (2.1)). We choose to compare explicitly to the $\rho(T)$ data of [37], which is shown in figure 6 (squares) at ambient pressure with the residual resistivity subtracted out, together with the corresponding $\rho^{\rm exp}_{\rm mag}(T)$ (circles) obtained by further subtracting the resistivity of $LaAl_3$. Figure 6 also shows corresponding results for $\rho^{\rm exp}_{\rm mag}(T)$ obtained at a pressure $P = 0.4$ GPa [38] (triangles), using the same sample as in [37]. The theoretical $\rho_{\rm mag}(T)$ is calculated and scaled onto the ambient pressure $\rho^{\rm exp}_{\rm mag}(T)$ in the usual way, leading thereby to a coherence scale of $\omega_L \simeq 33$ K. From figure 6, comparison between theory and experiment is seen to be good up to $T \simeq 45$ K, beyond which the experimental $\rho^{\rm exp}_{\rm mag}(T)$ drops much more rapidly with further increasing T. This is natural, for inelastic

neutron scattering experiments [40] show two higher crystal field levels occurring at almost the same energy, 6.1 meV (70.8 K) and 6.4 meV (74.2 K) above the ground state. Marked in figure 6, these are accessed thermally as T approaches $\sim$70 K, and provided they couple effectively to the conduction band (as appears to be the case here) the two additional conduction channels diminish the resistivity significantly.

We now comment briefly on the high pressure magnetic resistivity shown in figure 6. The coherence scale $\omega_{\rm L} = ZV^2$ itself naturally varies with pressure, but in the strongly correlated Kondo lattice regime the T-dependence of the magnetic resistivity should depend universally on $T/\omega_{\rm L}$ alone (section 2). The same theoretical $\rho_{\rm mag}(T)$ employed for comparison to the ambient pressure data should thus, with mere rescaling of the axes, account for $\rho^{\rm exp}_{\rm mag}(T)$ at $P = 0.4$ GPa (again up to the temperature at which the CEF excitations kick in). That indeed it does is shown in figure 6 (dashed line), the resultant coherence scale being found to be $\omega_{\rm L}$ ($P = 0.4$ GPa) $\simeq 71$ K.

Finally we turn to the optical conductivity, the experimental results [35] shown in figure 7 (top panel) being obtained from reflectance spectroscopy (lines) and surface impedance measurements (points). The bottom panel shows the theoretical $\sigma(\omega; T)$ obtained with the bare parameters specified above, converted to cm^{-1} using $\omega_{\rm L} = 33$ K inferred above from static transport. The theory evidently captures the unusual optical characteristics of $CeAl_3$, and agreement with experiment is seen to be rather good. A strong Drude peak, and a very shallow pseudogap, are seen at the lowest temperatures in theory and experiment, the Drude absorption collapsing on a temperature scale of $\sim$10 K, above which very little T dependence is found across the entire frequency range. Most significantly, no distinct direct gap/mIR peak arises, the spectrum being largely featureless (the small feature visible at $\sim 10^4$ cm^{-1} in the theoretical $\sigma(\omega; T)$ occurs on the effective bandwidth scale, and its intensity diminishes further with increasing U). The nominal location of the direct gap itself can however be determined theoretically from the renormalized band structure underlying the present theory (as considered in I, see figure 11). It is found to lie at $\omega \sim 10^3$ cm^{-1} as marked in figure 7, albeit that no sharp absorption occurs in its vicinity.

6. $CeCoIn_5$

This recently discovered [43], moderately heavy fermion compound crystallizes in a tetragonal structure consisting of alternate layers of $CeIn_3$ and $CoIn_2$. It superconducts below $T_{\rm c} \simeq 2.3$ K (the highest transition temperature of all known HF systems at ambient pressure [43]), and is paramagnetic for $T > T_{\rm c}$. The experimental resistivities $\rho(T)$ determined by four different groups [43–46] are shown in figure 8. That they differ widely presumably reflects intrinsic difficulties in measuring the dimensions of relatively small samples. Their basic equivalence is however seen by taking the results of one as a reference and rescaling the y-axis for each of the remaining data sets. With this, as shown in the inset to figure 8, all four resistivities collapse to essentially a common form (that of [46] deviating just slightly at higher T). These differences are nonetheless potentially significant when comparing to theory, for which the magnetic contribution $\rho^{\rm exp}_{\rm mag}(T)$ is required, obtained as in equation (2.1) by subtracting the resistivity of the non-magnetic $LaCoIn_5$. The results in figure 8 show that the a factor in equation (2.1)—the relative weight of $\rho(T)$ compared to that for the non-magnetic homologue—could vary by a factor of up to four or so, and is not therefore known with confidence.

Figure 9 shows the experimental $\rho^{\rm exp}_{\rm mag}(T)$ (open circles) determined in [44] by subtracting the resistivity of $LaCoIn_5$ from that for $CeCoIn_5$, corresponding as such to $a = 1$ (or equivalently, if e.g. $\rho(T)$ from [45] had been used instead, to an a of $\sim$2). To compare to theory we consider the parameters $\epsilon_{\rm c} = 0.5$ and $\eta = 0$, with $U = 3.75$ and $V^2 = 0.8$ (corresponding to

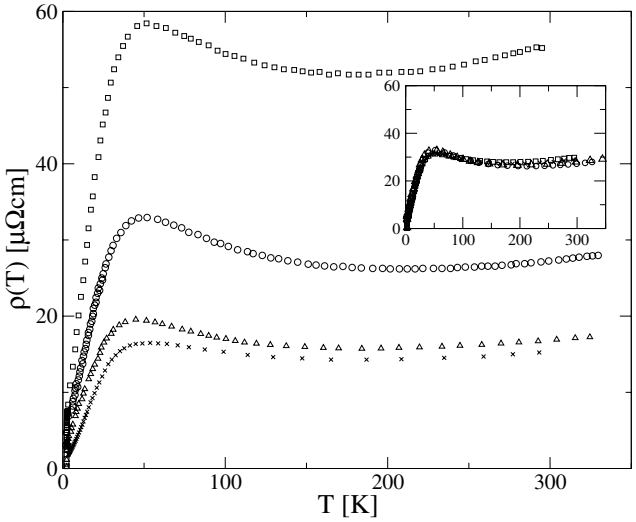

Figure 8. Experimental resistivity of $CeCoIn_5$ measured by different groups: [44] (circles), [46] (squares), [43] (triangles) and [45] (crosses). Inset: showing collapse of experimental resistivities to common form on rescaling the y-axis alone.

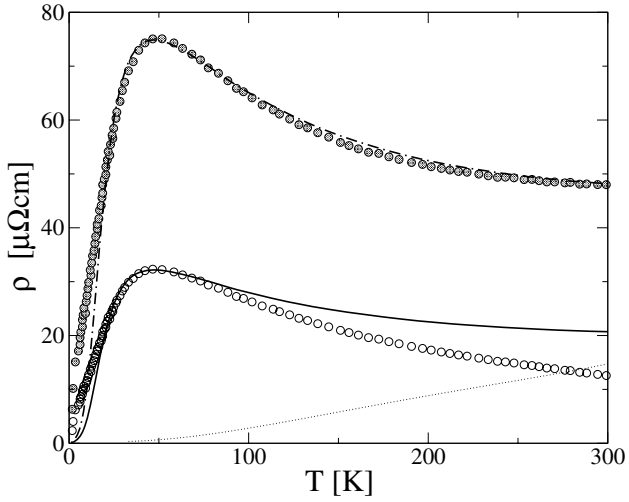

Figure 9. $CeCoIn_5$. Open circles denote the experimental $\rho^{\rm exp}_{\rm mag}(T)$ from [44], corresponding to $a = 1$ in equation (2.1) (the dotted line shows the resistivity of $LaCoIn_5$). The solid line shows the theoretical $\rho_{\rm mag}(T)$ for the bare parameters described in the text, with coherence scale $\omega_{\rm L} = 60$ K. Filled circles denote an experimental $\rho^{\rm exp}_{\rm mag}(T)$ obtained with $a = 2.3$ instead; the corresponding theoretical $\rho_{\rm mag}(T)$ (again with $\omega_{\rm L} = 60$ K) is now shown as a point–dash line. Full discussion in text.

an intermediate coupling strength $U/\pi\,\Delta_0 \simeq 1$). The resultant theoretical $\rho_{\rm mag}(T)$ is compared to experiment in figure 9 (solid line), yielding a coherence scale of $\omega_{\rm L} = 60$ K. It matches $\rho^{\rm exp}_{\rm mag}(T)$ for 15 K $\lesssim T \lesssim$ 100 K, the deviation at low temperatures presumably reflecting the approach to the superconducting state. The deviation above $T \simeq 100$ K also appears natural, since a direct determination of the CEF energy level scheme from inelastic neutron

scattering [47] shows an excited level at 8.6 meV or ∼100 K (with a second at a much higher energy, 24.4 meV), the extra conduction channel acting to diminish $\rho^{\rm exp}_{\rm mag}(T)$ more rapidly than the one-channel theory.

Our guess is that the latter inference is correct, at least qualitatively. A degree of caution is however required, since this is sensitive to a change in the value of a. To illustrate this, figure 9 also shows a new $\rho^{\rm exp}_{\rm mag}(T)$ (filled circles) obtained with $a = 2.3$ in equation (2.1). The theoretical $\rho_{\rm mag}(T)$ with the same coherence scale $\omega_{\rm L} = 60$ K, but with the overall y-axis naturally increased by factor of 2.3, now describes $\rho^{\rm exp}_{\rm mag}(T)$ very well for essentially all $T \gtrsim 15$ K. The quantitative influence of the extra conduction channel can thus be assessed with confidence only if the relative values of the resistivity for the magnetic and non-magnetic compounds are known accurately, although we add that the inferred low temperature coherence scale $\omega_{\rm L} = 60$ K is not itself sensitive to a.

We turn now to the optical conductivity. Experimental results from reflectivity measurements [45] are shown in figure 10 (top panel), with the ω-dependence on a log scale up to $\omega = 30$ cm^{-1} and a linear scale thereafter (separated by a vertical line). For $\omega < 30$ cm^{-1} the results are extrapolated (dashed lines) towards the dc limit [45], as required for the Kramers–Krönig analysis of the reflectivity that leads to the experimental $\sigma(\omega; T)$ shown. The theoretical $\sigma(\omega; T)$ is shown in the lower panel, for the bare parameters specified above, with $\omega_{\rm L} = 60$ K.

The comparison between theory and experiment is at least qualitatively satisfactory, albeit not as good as for $YbAl_3$ or $CeAl_3$ (perhaps unsurprisingly given the quasi-2D nature of $CeCoIn_5$). The pseudogap at $T = 10$ K is seen to lie at ∼65 cm^{-1}, and as in experiment shifts gradually to higher ω with increasing temperature and fills up progressively—on the scale of ∼1–2$\omega_{\rm L}$ or ∼60–120 K. The direct gap absorption in theory and experiment lies at $\Delta_{\rm dir} \sim 600$ cm^{-1}, and starts to lose spectral weight significantly for $T \gtrsim 50$ K or so, i.e. on the scale of $\omega_{\rm L}$ itself. This suggests that $CeCoIn_5$ is not in the strong coupling, Kondo lattice regime, since in strong coupling the direct gap/mIR absorption is significantly eroded for temperatures approaching the order of the direct gap itself (∼600 cm^{-1} or ∼900 K in the present case), see e.g. figure 12 of I. For $CeCoIn_5$ by contrast, significant thermal erosion is seen to occur for $T \gtrsim 50$ K $\sim \Delta_{\rm dir}/20$, which behaviour is typical of intermediate coupling strengths. This also appears to be consistent with dHvA measurements [48], which yield a moderate effective mass m^* in the range ≃10–20.

Two further points should be mentioned. First, the $\omega \lesssim 30$ cm^{-1} values of the theoretical $\sigma(\omega; T)$ are clearly lower than the experimental extrapolations. As $\omega \to 0$, the latter extrapolate to the dc conductivity obtained in [45]. The dc limit of the theoretical $\sigma(0; T)$ by contrast gives the $1/\rho_{\rm mag}(T)$ shown in figure 9 (solid line), and aside from the $T = 292$ K case this agrees well with the experimental dc conductivity of [44]—which as seen from figure 8 differs by a factor of two or so from that of [45]. The issue here appears largely to be experimental, reflecting the significant difference between the resistivities of [44] and [45]. Second, the vertical arrows at $\omega \simeq 250$ cm^{-1} in the experimental $\sigma(\omega; T)$ of figure 10 indicate weak additional absorption that has been ascribed [45] to a Holstein band due to coupling to a bosonic mode. This is not of course included in the present theory, which thus shows somewhat less absorption in the region.

7. Conclusion

We have here employed a local moment approach to the periodic Anderson lattice developed in I, to make direct comparison to dc transport and optical conductivities of CeB_6, $YbAl_3$, $CeAl_3$ and $CeCoIn_5$. The Yb compound is a representative intermediate valence material, and

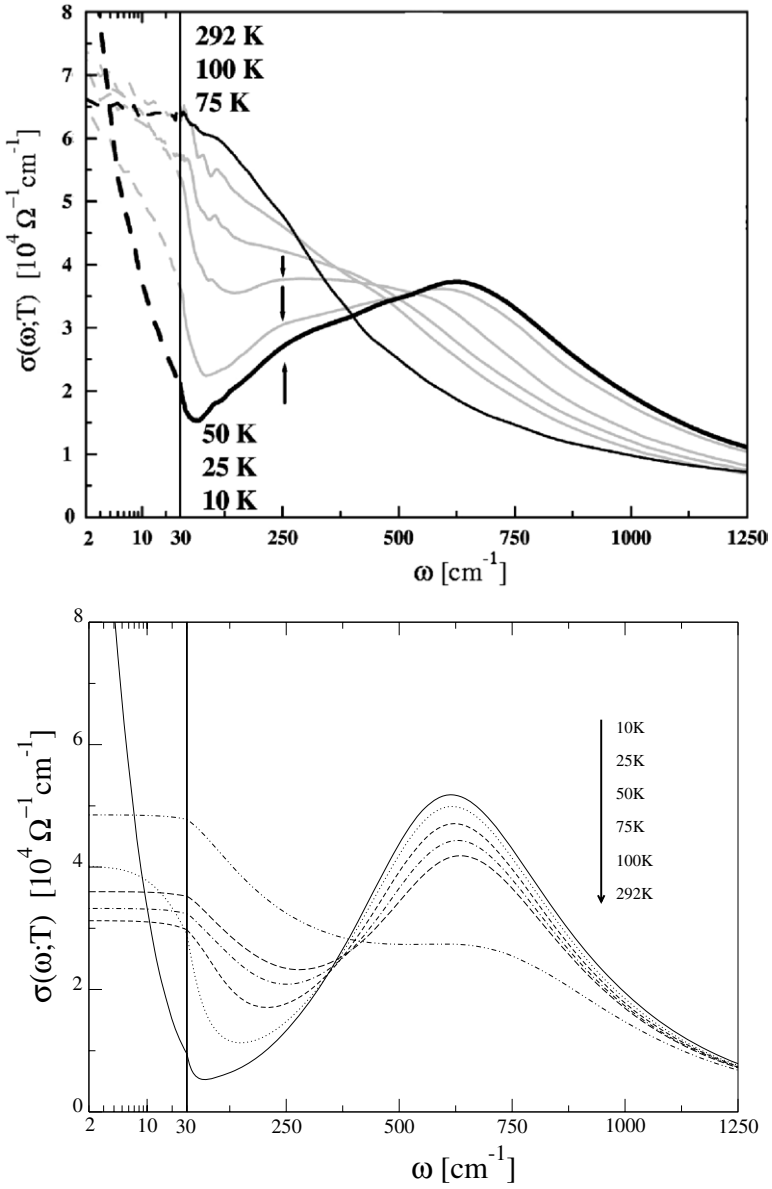

Figure 10. Top panel: experimental optical conductivity of $CeCoIn_5$ at various temperatures [45]. Bottom panel: corresponding theoretical $\sigma(\omega; T)$ obtained for the parameter set $\epsilon_c = 0.5$, $\eta = 0$, $U = 3.75$ and $V^2 = 0.8$, with $\omega_L = 60$ K ($\sim$42 cm^{-1}). In both cases the frequency axis is logarithmic up to $\omega = 30$ cm^{-1} and linear thereafter (separated by a vertical line). Full discussion in text.

the others typify heavy fermion behaviour, from the strongly correlated Kondo lattice regime appropriate to $CeAl_3$ and CeB_6 to what we believe is the somewhat weaker coupling case of $CeCoIn_5$. In broad terms more or less all characteristic features of the optics and transport of these materials are captured, the natural exception, omitted from the model itself, being crystal field effects which may (or may not) show up in the experimental resistivity as a reduction

below one-channel behaviour at suitably high temperatures. The theory in general performs rather well quantitatively, and also captures notable features specific to individual systems, for example the existence of a low-frequency shoulder observed in the optics of $YbAl_3$ [31], or the absence of any significant direct gap/mIR absorption in $CeAl_3$ [35].

Minimalist though it is, the underlying model, and the theory for it, thus appear to provide quite a comprehensive and successful description of experiment. This we attribute in no small part both to the dominance of the local electron scattering inherent to the model itself, and the need to provide an adequate theoretical description of such on all experimentally relevant frequency and temperature scales.

Acknowledgments

We are grateful to the following for permission to quote their experimental results: L Degiorgi, H Okamura, G Oomi and F Steglich. We express our thanks to the EPSRC for supporting this research.

References

[1] Grewe N and Steglich F 1991 *Handbook on the Physics and Chemistry of Rare Earths* vol 14, ed K A Gschneider Jr and L L Eyring (Amsterdam: Elsevier) p 343
[2] Hewson A C 1993 *The Kondo Problem to Heavy Fermions* (Cambridge: Cambridge University Press)
[3] Aeppli G and Fisk Z 1992 *Comments Condens. Matter Phys.* **16** 155
[4] Fisk Z *et al* 1996 *Physica* B **223/224** 409
[5] Takabatake T *et al* 1998 *J. Magn. Magn. Mater.* **177–181** 277
[6] Degiorgi L 1999 *Rev. Mod. Phys.* **71** 687
[7] Riseborough P S 2000 *Adv. Phys.* **49** 257
[8] Vollhardt D 1993 *Correlated Electron Systems* vol 9, ed V J Emery (Singapore: World Scientific)
[9] Pruschke T, Jarrell M and Freericks J K 1995 *Adv. Phys.* **44** 187
[10] Georges A, Kotliar G, Krauth W and Rozenberg M 1996 *Rev. Mod. Phys.* **68** 13
[11] Gebhard F 1997 *The Mott Metal–Insulator Transition* (*Springer Tracts in Modern Physics*) vol 137 (Berlin: Springer)
[12] Logan D E and Vidhyadhiraja N S 2005 *J. Phys.: Condens. Matter* **17** 2935
[13] Vidhyadhiraja N S and Logan D E 2004 *Eur. Phys. J.* B **39** 313–34
[14] Smith V E, Logan D E and Krishnamurthy H R 2003 *Eur. Phys. J.* B **32** 49
[15] Vidhyadhiraja N S, Smith V E, Logan D E and Krishnamurthy H R 2003 *J. Phys.: Condens. Matter* **15** 4045–87
[16] Strong S P and Millis A J 1994 *Phys. Rev.* B **50** 12611
[17] Kashiba S, Maekawa S, Takahashi S and Tachiki M 1986 *J. Phys. Soc. Japan* **55** 1341
[18] Cornut B and Coqblin B 1972 *Phys. Rev.* B **5** 4541
[19] Yamada K, Yosida K and Hanzawa K 1984 *Prog. Theor. Phys.* **71** 450
[20] Suzuki H, Kitazawa H, Naka T, Tang J and Kido G 1998 *Solid State Commun.* **107** 447
[21] Gorshunov B, Sluchanko N, Volkov A, Dressel M, Knebel G, Loidl A and Kunii S 1999 *Phys. Rev.* B **59** 1808
[22] Sato N, Sumiyama A, Kunii S, Nagano H and Kasuya T 1985 *J. Phys. Soc. Japan* **54** 1923–32
[23] Kimura S, Nanba T, Kunii S and Kasuya T 1994 *Phys. Rev.* B **50** 1406
[24] Nakamura S, Goto T and Kunii S 1995 *J. Phys. Soc. Japan* **64** 3941–5
[25] Goodrich R G *et al* 2004 *Phys. Rev.* B **69** 054415
[26] Marcenat C, Jaccard D, Sierro J, Flouquet J, Onuki Y and Komatsubahara T 1990 *J. Low Temp. Phys.* **78** 261
[27] Zirngiebl E *et al* 1984 *Phys. Rev.* B **30** 4052
[28] Ohara S, Chen G F and Sakamoto I 2001 *J. Alloys Compounds* **323/324** 632–5
[29] Schweitzer H and Czycholl G 1991 *Phys. Rev. Lett.* **67** 3724
[30] Ebihara T *et al* 2000 *J. Phys. Soc. Japan* **69** 895
[31] Okamura H, Michizawa T, Nanba T and Ebihara T 2004 *J. Phys. Soc. Japan* **73** 2045
[32] Cornelius A L *et al* 2002 *Phys. Rev. Lett.* **88** 117201
[33] Suga S *et al* 2002 *Abstr. Fall Meet. Physical Society of Japan* 7aXC-6
[34] Rowe D M, Kuznetsov V L, Kuznetsova L A and Min G 2002 *J. Phys. D: Appl. Phys.* **35** 2183–6
[35] Awasthi A M, Degiorgi L, Grüner G, Dalichaouch Y and Maple M B 1993 *Phys. Rev.* B **48** 10692

[36] Riseborough P S 2003 *Phys. Rev.* B **67** 045102
[37] Kagayama T, Munakata K and Oomi G 1993 *J. Alloys Compounds* **192** 239–41
[38] Oomi G and Kagayama T 1996 *J. Phys. Soc. Japan* **65** 2732–3
[39] Andres K, Graebner J E and Ott H R 1975 *Phys. Rev. Lett.* **35** 1779
[40] Goremychkin E A, Osborn R and Sashin I L 1999 *J. Appl. Phys.* **85** 6046
[41] Jaccard D, Cibin R and Sierro J 1988 *Helv. Phys. Acta* **61** 530–7
[42] Jaccard D and Flouquet J 1985 *J. Magn. Magn. Mater.* **47/48** 45–50
[43] Petrovic *et al* 2001 *J. Phys.: Condens. Matter* **13** L337–42
[44] Nakatsuji S *et al* 2002 *Phys. Rev. Lett.* **89** 106402
[45] Singley E J, Basov D N, Bauer E D and Maple M B 2002 *Phys. Rev.* B **65** 161101
[46] Nicklas M *et al* 2001 *J. Phys.: Condens. Matter* **13** L905–12
[47] Bauer E D *et al* 2004 *J. Appl. Phys.* **95** 7201
[48] Hall D *et al* 2001 *Phys. Rev.* B **64** 212508